IEEE Access
Multidisciplinary ⋮ Rapid Review ⋮ Open Access Journal

Received November 26, 2019, accepted December 18, 2019, date of publication January 14, 2020, date of current version February 14, 2020.

Digital Object Identifier 10.1109/ACCESS.2020.2966580

Road Detection Based on Shearlet for GF-3 Synthetic Aperture Radar Images

ZENGGUO SUN[1,2], DEDAO LIN[2], WEI WEI[3], (Senior Member, IEEE), MARCIN WOŹNIAK[4], AND ROBERTAS DAMAŠEVIČIUS[5]

[1]Key Laboratory of Modern Teaching Technology, Ministry of Education, Xi'an 710062, China
[2]School of Computer Science, Shaanxi Normal University, Xi'an 710119, China
[3]School of Computer Science and Engineering, Xi'an University of Technology, Xi'an 710048, China
[4]Institute of Mathematics, Silesian University of Technology, 44-100 Gliwice, Poland
[5]Multimedia Engineering Department, Faculty of Informatics, Kaunas University of Technology, 44249 Kaunas, Lithuania

Corresponding author: Wei Wei (weiwei@xaut.edu.cn)

This work was supported in part by the National Natural Science Foundation of China under Grant 61102163, Grant 61703096, and Grant 41471280, in part by the Fundamental Research Funds for the Central Universities under Grant GK201903085, and in part by the Key Research and Development Program of Shaanxi Province under Grant 2018ZDXM-GY-036.

ABSTRACT GF-3 satellite is China's first C-band multi-polarized synthetic aperture radar (SAR) satellite with the 1-meter resolution, which has been widely used in various fields. Road detection for GF-3 SAR images is an important part of the application of GF-3, especially in fields of map update, target recognition, and image matching. However, speckle appears in GF-3 SAR images due to coherent imaging system and it hinders the interpretation of images seriously. Especially the detection of weak roads under strong speckle background becomes extremely difficult. As a representative of multiscale geometric analysis (MGA) tool, shearlet has the optimal sparse representation feature and strong directional orientation, which can effectively capture edge and other anisotropic feature information, and can accurately describe the sparse characteristics of GF-3 SAR images. Based on shearlet, a method for detecting weak roads under strong speckle interference is proposed. Firstly, the Frost filter is used for despeckling. Secondly, shearlet is used for road detection. Finally, morphological operations are adopted to obtain the final result. Road detection experiments on various types of GF-3 SAR images demonstrate that, the proposed method can effectively overcome the interference of speckle, and completely and smoothly detect road information, which is very suitable for the detection of weak roads under strong speckle interference of GF-3 SAR images.

INDEX TERMS GF-3 synthetic aperture radar images, road detection, shearlet, morphological operation.

I. INTRODUCTION

GF-3 satellite is China's first C-band multi-polarized synthetic aperture radar (SAR) satellite with the 1-meter resolution. It can penetrate clouds and rain areas, not limited by day and night, penetrate vegetation, and go deep into the ground. It is widely used in agriculture, disaster monitoring, geology, lakes, marine monitoring and navigation, etc. Like ground targets such as airports, bridges, dams and rivers, roads in GF-3 SAR images are not only strategically important in military but also important for the development of the national economy.

Speckle appears in GF-3 SAR images due to coherent imaging system and it hinders the interpretation of images seriously [1]. Appearance of speckle makes road detection extremely difficult, especially the detection of weak roads under strong speckle interference. This makes the traditional edge detectors based on difference operators invalid for SAR images such as Sobel, LoG and Canny [2], [3]. These traditional edge detectors usually result in a lot of false edges for SAR images. These false edges cover up real edges and reduce accuracy of edge detection. Recently, there are some novel edge detectors presented in references, such as [4], [5] and [6]. In [5], the author proposed a novel robust edge detector. In [6], the author proposed a SAR phase congruency detector (SAR-PC). It should be noted that GF-3 SAR images usually own strong sparsity [7], [8]. But the traditional difference-based edge detectors and the two new detectors above do not take into account the sparsity of images. In [4], the author proposed a new SAR image detection algorithm based on the de-noising algorithm via the shearlet-based sparse representation and a new morphology edge detector.

The associate editor coordinating the review of this manuscript and approving it for publication was Dimitris E. Anagnostou.

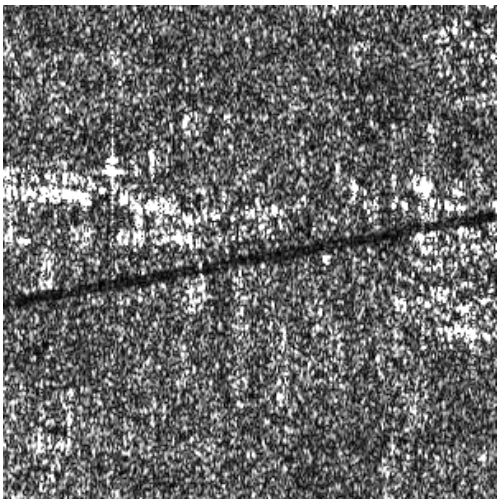

FIGURE 1. Road of GF-3 SAR image.

Motivated by this idea, the use of sparsity of GF-3 SAR images is focused in this paper, which is helpful to obtain high accuracy of road detection.

In recent years, multi-scale geometric analysis (MGA) tools have been widely used in the field of image processing. Among these tools, shearlet has optimal sparsity and complete mathematical theory. Compared with other wavelet tools, shearlet is more suitable for processing geometric features in multi-dimensional data. It has strong directional orientation and can effectively capture edge and other anisotropic feature information. Therefore, we use shearlet, the optimal sparse tool, to perform road detection on GF-3 SAR images, which can better suppress speckle, improve detection accuracy, and obtain smooth and continuous road detection results.

The weak roads under strong speckle interference are detected in this paper. Due to the interference of speckle in GF-3 SAR images, the Frost filter is used for despeckling, which can reduce the impact of speckle on the subsequent road detection. Then, shearlet is used for road detection to get high detecting accuracy. Finally, morphological operations are adopted to refine edges and eliminate false edges to obtain the final result. Road detection experiments on different types of GF-3 SAR images verify the effectiveness of the proposed method.

II. GF-3 SAR IMAGES

GF-3 satellite is a C-band and multi-polarized SAR satellite with the highest resolution in the world. In addition, it is also China's first low-orbit remote sensing satellite with a design life of 8 years. It can provide users with long-term and stable data support services. It also improves the efficiency of the satellite system and has a wide range of applications in various fields. Figure 1 shows a scene of a GF-3 SAR image with a road and the corresponding imaging parameters are shown in Table 1. In this image, there is a lot of strong speckle and the road shows weak gray, so the speckle seriously interferes with the detection of the roads. For the detection of weak roads under such strong speckle interference, the traditional difference operators fail. Because GF-3 SAR images have strong sparsity, and shearlet has the optimal sparsity and strong directional orientation, we use shearlet to perform road detection for GF-3 SAR images [9]–[19].

TABLE 1. The parameters of GF-3 SAR image.

Ground receiving station	Imaging mode	Polarization	Resolution	Imaging position
Miyun Station	FSII	HHHV	10m	E109.6 N35.1

III. SHEARLET

This section introduces the definition, the optimal sparsity and the strong directional orientation of shearlet and provides sufficient theoretical basis for the road detection [20]–[31].

A. INTRODUCTION

Shearlet is a new multi-scale geometric analysis method based on the theory of traditional affine system. It is constructed by a special form of affine system with compound expansion. When dimension $n = 2$, the affine system with compound expansion is defined as [32], [33]

$$\Psi_{AB}(\psi) = \left\{\psi_{j,l,k}(x) = |\det A|^{j/2}\,\psi\left(B^l A^j x - k\right) : j, l \in \mathbf{Z},\ k \in \mathbf{Z}^2\right\}, \quad (1)$$

where $\psi \in L^2(\mathbf{R}^2)$, j, l and k are scale, shear and translation parameters, A and B are invertible matrices, $|\det B| = 1$, A^j is a scale transformed matrix, B^l is associated with a geometric transformation that maintains an area constant such as rotation and shear transformation. When $S_k = \begin{pmatrix} 1 & k \\ 0 & 1 \end{pmatrix}$ is the anisotropic expansion matrix and $B = B_0 = \begin{pmatrix} 1 & 1 \\ 0 & 1 \end{pmatrix}$ is the shear matrix, the equation above becomes shearlet. For each $(\xi_1, \xi_2) \in \mathbf{D}_0$, there is

$$\sum_{j\geq 0}\sum_{l=-2^j}^{2^j-1}\left|\hat{\psi}^{(0)}\left(\xi A_0^{-j}B_0^{-l}\right)\right|^2 = \sum_{j\geq 0}\sum_{l=-2^j}^{2^j-1}\left|\hat{\psi}_1\left(2^{-2j}\xi_1\right)\right|^2\left|\hat{\psi}_2\left(2^j\frac{\xi_2}{\xi_1} - l\right)\right|^2 = 1, \quad (2)$$

where $\mathbf{D}_0 = \left\{(\xi_1, \xi_2) \in \hat{\mathbf{R}}^2 : |\xi_1| \geq 1/8,\ \left|\xi_2/\xi_1\right| \leq 1\right\}$. The function $\left\{\hat{\psi}^{(0)}\left(\boldsymbol{\xi} A_0^{-j}B_0^{-l}\right)\right\}$ is a split of $\mathbf{D}_0$, which is shown in Figure 2(a). Because the set

$$\left\{\psi^{(0)}_{j,l,k}(x) = 2^{\frac{3j}{2}}\psi^{(0)}\left(B_0^l A_0^j x - k\right) : j \geq 0,\ -2^j \leq l \leq 2^j - 1,\ k \in \mathbf{Z}^2\right\}, \quad (3)$$

is a Parseval frame of $L^2(\mathbf{D}_0)^\vee = \left\{f \in L^2(\mathbf{R}^2) : \operatorname{supp}\hat{f} \subset \mathbf{D}_0\right\}$, it is easy to find that the function $\psi_{j,l,k}$ has

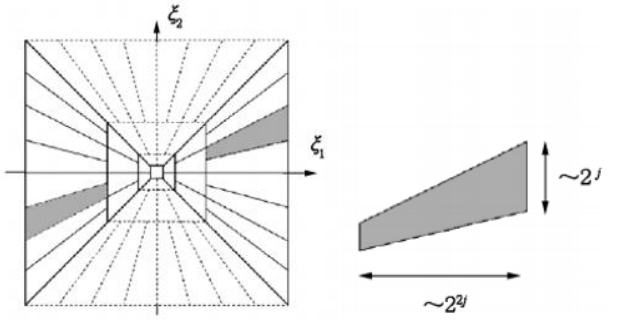

FIGURE 2. Spatial-frequency plane and frequency support of shearlet: (a) Frequency domain split of shearlet, (b) Frequency domain support of shearlet.

the following frequency domain support [34]

$$\begin{aligned}&\operatorname{supp} \hat{\psi}_{j,l,k}^{(0)}\\ &\subset \left\{(\xi_1,\xi_2):\xi_1\in\left[-2^{2j-1},-2^{2j-4}\right]\cup\left[2^{2j-4},2^{2j-1}\right],\right.\\ &\left.\left|\xi_2\Big/\xi_1+l2^{-j}\right|\le 2^{-j}\right\}.\end{aligned}\tag{4}$$

It means that each element $\hat{\psi}_{j,l,k}$ is supported by the trapezoid whose approximate size is $2^{2j}\times 2^j$, and whose direction is along with the line with the slope $l2^{-j}$(Shown in Figure 2(b)). It can be seen that shearlet has great local characteristics and strong directional sensitivity.

B. THE OPTIMAL SPARSE REPRESENTATION OF THE SHEARLET

Denoting f as the function that the direction is C^2 except a curve that is piecewise C^2 continuous respectively. f_N^S is the approximation of the maximum shearlet coefficient that the count is N of f. The relationship between them is [35]

$$\left\|f-f_N^s\right\|_2^2\le CN^{-2}\left(\log N\right)^3.\tag{5}$$

From the formula, we can see that the approximation order of shearlet can be reached $O\left(N^{-2}\left(\log N\right)^3\right)$. Compared with other multi-scale geometric analysis tools, shearlet has optimal sparsity and can optimally represent images in various directions and scales. For GF-3 SAR images with obvious sparsity, using shearlet, an optimal sparse tool, can lead to an ideal road detection result.

IV. DETECTION STEPS

The weak roads under strong speckle interference are detected in this paper. This section firstly uses the Frost filter to preprocess SAR images. This can mitigate the interference of speckle on road detection. Then, shearlet with optimal sparsity is used to perform road detection. Finally, morphological operations are adopted to refine edges and eliminate false edges to obtain an ideal result.

A. FROST FILTER PREPROCESSING

Because we mainly study the weak roads under strong speckle interference in GF-3 SAR images, it is necessary to choose a suitable filter to suppress speckle, reduce the false edges on the road detection, and effectively retain the road feature information to be detected. Since the Frost filter [36] is an algorithm that preserves edges and fine details well in the traditional speckle reduction algorithms, this section uses the Frost filter to smooth speckle effectively. And we can get a to-be-processed image in which speckle is effectively suppressed and road information is effectively retained.

The Frost filter is defined as

$$\hat{R}_{kl}=\frac{\sum_i\sum_j P_{ij}m_{ij}}{\sum_i\sum_j m_{ij}},\quad m_{ij}=e^{-\eta C_I^2 d_{ij}}.\tag{6}$$

where $\hat{R}_{kl}$ represents the filtered output of the center pixel (k,l), P_{ij} is the gray value of any pixel in the sliding window, d_{ij} is the distance from any pixel in the sliding window to the central pixel, C_I is the coefficient of variation that is defined by the ratio of the sample standard deviation to the sample mean, and η ($\eta > 0$) is the tuning factor. The larger the value of η, the stronger the ability to maintain the edge, and conversely, the stronger the ability to suppress the speckle.

From (6), C_I has a direct impact on the performance of the Frost filter. When C_I is small, the Frost filter can suppress speckle more sufficiently in homogeneous regions. When C_I is larger, the Frost filter can effectively preserve edge information in edge regions. Therefore, C_I is a measure that reflects the adaptability of the Frost filtering. In addition, the Frost filter assigns different weight values to pixels at different positions in the sliding window. The farther away from the central pixel, the smaller the weight, which tends to preserve the edge and detail information of the image.

The Frost filter can sufficiently suppress the speckle in the homogeneous region and effectively preserve the edge information in the edge region. Therefore, we choose the Frost filter to preserve valid road information and suppress speckle as much as possible.

B. LOGARITHMIC TRANSFORMATION

The commonly used multiplicative speckle model of SAR images is defined as [37]

$$Y=FX,\tag{7}$$

where Y is an observed image, F is the speckle, and X is an real image.

Since shearlet is based on the additive speckle model, it is necessary to first make the above multiplicative model additive by using log-transform before using the shearlet transformation, i.e.,

$$\log\left(Y\right)=\log\left(\mathrm{F}\right)+\log\left(\mathrm{X}\right).\tag{8}$$

C. ROAD DETECTION BASED ON SHEARLET

The core of road detection is the edge detection based on phase congruency and shearlet. Phase congruency is an edge detection algorithm originally using Fourier coefficients. Because shearlet has the optimal sparse representation feature and strong directional orientation, in this section, we combine

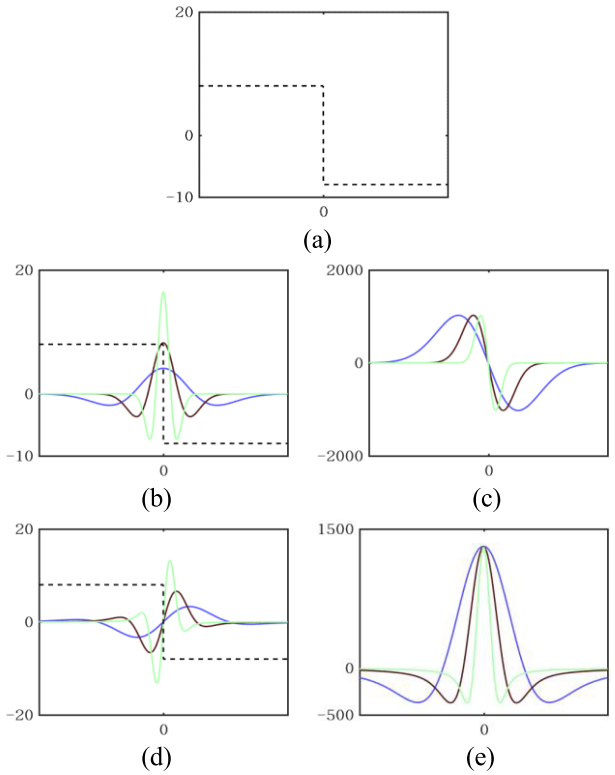

FIGURE 3. The principle of edge detection on one dimension. (a) An ideal edge on one dimension. (b) $\psi_{j,0}^{even}$, the even-symmetric wavelets centered on the edge with different scale parameters. (c) A graph of the wavelet coefficients of the even-symmetric wavelets with different scale parameters at different positions. The horizontal axis is the shift x and the vertical axis is the value of $\left\langle f, \psi_{j,x}^{even} \right\rangle$. (d) $\psi_{j,0}^{odd}$, the odd-symmetric wavelets centered on the edge with different scale parameters. (e) A graph of the wavelet coefficients of the odd-symmetric wavelets with different scale parameters at different positions. The horizontal axis is the shift x and the vertical axis is the value of $\left\langle f, \psi_{j,x}^{odd} \right\rangle$.

phase congruency and shearlet together. In order to facilitate understanding, we first introduce edge detection on one dimension which is regarded as the simulation of theoretical background of our method, then we provide the case of two dimensions. The principle is described as follows [2], [38].

1) EDGE DETECTION ON ONE DIMENSION

We define a wavelet system as $\psi_{j,x}$, where $j\,(j > 0)$ is the scale parameter, x is the translation parameter and $x \in \mathbb{R}$. $\psi_{j,x}^{even}$ represents an even-symmetric wavelet and $\psi_{j,x}^{odd}$ represents an odd-symmetric wavelet. f represents a one-dimension signal and the inner product $\langle f, \psi_{j,x} \rangle$ represents the wavelet coefficient at the position x. The principle of edge detection on one dimension is shown in Figure 3.

We use phase congruency with the even-symmetric wavelets which contain different parameters on an ideal edge. Then we find that $\left\langle f, \psi_{j,x}^{even} \right\rangle = 0$ for all $j > 0$ when the even-symmetric wavelets are centered on the edge. As the dilated wavelets are shifted away from the edge, the inner product increases or decreases rapidly away from zero. We use phase congruency with the odd-symmetric wavelets which contain different parameters on an ideal edge. Then we find that $\left\langle f, \psi_{j,x}^{odd} \right\rangle$ is constant, nonzero and achieves a local maximum at $x = 0$ for all $j > 0$ when the odd-symmetric wavelets are centered on the edge. As they are shifted away from the edge, the value of the inner product drops rapidly from that maximum. We can use these properties to judge whether a pixel is part of an edge on one dimension. The probability of each pixel which is part of an edge is between 0 and 1. If the probability is 0, it means there is no edge. If the probability is 1, it means there must be en edge here.

The calculation formula for the probability that each pixel exists on the edge is

$$\tilde{E}_{\psi^{even},\psi^{odd}}(f,x) = \frac{\left|\sum_{i=1}^{I} \left\langle f, \psi_{j_i,x}^{odd} \right\rangle\right| - \sum_{i=1}^{I} \left|\left\langle f, \psi_{j_i,x}^{even} \right\rangle\right|}{I \cdot \max\limits_{i\in\{1,2,3,\ldots,I\}} \left|\left\langle f, \psi_{j_i,x}^{odd} \right\rangle\right| + \varepsilon}, \quad (9)$$

where $\varepsilon > 0$ prevents division by zero, $I \in \{1, 2, \ldots\}$ is the number of scale parameters.

$\tilde{E}_{\psi^{even},\psi^{odd}}(f,x)$ may be less than 0. To ensure that the probability value of each pixel is between 0 and 1, the formula is defined as

$$E_{\psi^{even},\psi^{odd}}(f,x) = \max\left(\tilde{E}_{\psi^{even},\psi^{odd}}(f,x), 0\right). \quad (10)$$

When the wavelet is centered on an ideal edge, we can see that

$$\frac{\left|\sum_{i=1}^{I} \left\langle f, \psi_{j_i,x}^{odd} \right\rangle\right| - \sum_{i=1}^{I} \left|\left\langle f, \psi_{j_i,x}^{even} \right\rangle\right|}{I \cdot \max\limits_{i\in\{1,2,3,\ldots,I\}} \left|\left\langle f, \psi_{j_i,x}^{odd} \right\rangle\right|} = \frac{\left|\sum_{i=1}^{I} \left\langle f, \psi_{j_i,x}^{odd} \right\rangle\right|}{I \cdot \max\limits_{i\in\{1,2,3,\ldots,I\}} \left|\left\langle f, \psi_{j_i,x}^{odd} \right\rangle\right|} = 1. \quad (11)$$

When detecting edges on two dimensions, we approximate the direction k^* of a potential edge. To get the value of k^* of a pixel, we find which pair of parameters (j, k) yields the largest coefficients of $\left\langle f, \psi_{j,k,x_0}^{odd} \right\rangle$ for a fixed x_0 over a fixed range of j and all of the k computed. Then we detect edges in the one dimension case in the preferred direction k^*.

2) EDGE DETECTION ON TWO DIMENSIONS

We construct even-symmetric shearlet as a tensor product of the Mexican hat wavelet and a Gaussian [39]. The formula of even-symmetric shearlet is defined as

$$\psi_{j,k,x}^{even}(y) = 2^{\frac{3j}{2}} \psi^{even}\left(S_k A_j (y - x)\right), \quad (12)$$

where $j \in \mathbb{N}_0$ is the scale parameter, $|k| < \left\lceil 2^{\frac{j}{2}} \right\rceil$ is the shear parameter, $x \in \mathbb{Z}^2$ is the translation parameter, $S_k = \begin{pmatrix} 1 & k \\ 0 & 1 \end{pmatrix}$ is the shear matrix and $A_j = \begin{pmatrix} 2^j & 0 \\ 0 & 2^{j/2} \end{pmatrix}$ is the anisotropic expansion matrix.

Hilbert transform [40] is used to convert even-symmetric shearlet into odd-symmetric shearlet. The formula of odd- symmetric shearlet is defined as

$$\psi_{j,k,x}^{odd}(y) = 2^{\frac{3j}{2}} \psi^{odd}\left(S_k A_j (y - x)\right). \tag{13}$$

Next, the best direction of the road that exists on each pixel is calculated. We set $j \in \{J_{\min}, \ldots, J_{\max}\}$, where $J_{\min}$ and $J_{\max}$ represent the minimum and maximum values of j respectively, f represents an image, $\left\langle f, \psi_{j,k,x}^{even} \right\rangle$ represents the even-symmetric shearlet coefficient at the position x, and $\left\langle f, \psi_{j,k,x}^{odd} \right\rangle$ represents the odd-symmetric shearlet coefficient at the position x. The best direction $k^*_{\psi^{even},\psi^{odd}}(f,x) \in \left\{-\left\lceil 2^{\frac{J_{\min}}{2}} \right\rceil, \ldots, \left\lceil 2^{\frac{J_{\min}}{2}} \right\rceil\right\}$ for a road that exists on a pixel point $x \in \mathbb{Z}^2$ is defined as

$$k^*_{\psi^{even},\psi^{odd}}(f,x) = \underset{\tilde{k} \in \left\{-\left\lceil 2^{\frac{J_{\min}}{2}} \right\rceil, \ldots, \left\lceil 2^{\frac{J_{\min}}{2}} \right\rceil\right\}}{\arg\max} \max_{\substack{j \in \{J_{\min}, \ldots, J_{\max}\}, \\ k \in \left\{-\left\lceil 2^{\frac{j}{2}} \right\rceil, \ldots, \left\lceil 2^{\frac{j}{2}} \right\rceil\right\}, \\ \left|\tilde{k} - k\left\lceil 2^{\frac{J_{\min}}{2}} \right\rceil \left\lceil 2^{\frac{j}{2}} \right\rceil^{-1}\right| \le \frac{1}{2}}} \left|\left\langle f, \psi_{j,k,x}^{odd} \right\rangle\right|. \tag{14}$$

The calculation formula for the probability that each pixel exists on the road is

$$\tilde{E}_{\psi^{even},\psi^{odd}}(f,x) = \frac{\left|\sum_{j=J_{\min}}^{J_{\max}} \left\langle f, \psi_{j,k_j,x}^{odd} \right\rangle\right| - \sum_{j=J_{\min}}^{J_{\max}} \left|\left\langle f, \psi_{j,k_j,x}^{even} \right\rangle\right| - (J_{\max} - J_{\min} + 1)\, T}{(J_{\max} - J_{\min} + 1) \max\limits_{j \in \{J_{\min}, \ldots, J_{\max}\}} \left|\left\langle f, \psi_{j,k_j,x}^{odd} \right\rangle\right| + \varepsilon}, \tag{15}$$

where $\varepsilon > 0$ prevents division by zero, T is a soft threshold applied for noise removal. From the Figure 3 and the equation (15), we can know that $\tilde{E}_{\psi^{even},\psi^{odd}}(f,x)$ may be less than 0 and $\tilde{E}_{\psi^{even},\psi^{odd}}(f,x)$ cannot be greater than 1. And k_j is defined as

$$k_j = \underset{\substack{k \in \left\{-\left\lceil 2^{\frac{j}{2}} \right\rceil, \ldots, \left\lceil 2^{\frac{j}{2}} \right\rceil\right\}, \\ \left|k^*_{\psi^{even},\psi^{odd}}(f,x) - k\left\lceil 2^{\frac{J_{\min}}{2}} \right\rceil \left\lceil 2^{\frac{j}{2}} \right\rceil^{-1}\right| \le \frac{1}{2}}}{\arg\max} \left|\left\langle f, \psi_{j,k,x}^{odd} \right\rangle\right|. \tag{16}$$

To ensure that the probability value of each pixel is between 0 and 1, we take $\tilde{E}_{\psi^{even},\psi^{odd}}(f,x)$ into the equation (10) to calculate $E_{\psi^{even},\psi^{odd}}(f,x)$. If $\tilde{E}_{\psi^{even},\psi^{odd}}(f,x)$ is less than 0, we regard $E_{\psi^{even},\psi^{odd}}(f,x)$ as 0. $E_{\psi^{even},\psi^{odd}}(f,x)$ is between 0 and 1, which indicates the likelihood of a road at the pixel x. Then, we make an exponential transformation of the image. Finally, we set a threshold and binarize the image to obtain the edge information of the GF-3 SAR image.

D. MORPHOLOGICAL OPERATION

Road detection based on shearlet can ensure the accuracy. But in the detection result, the edges are thick, and there are still a few false edges. Therefore, two morphological operations are used to further optimize the road result detected by shearlet in this section, including refinement and removal of false edges.

Mathematical morphology is composed of a set of morphological algebraic operators. It has four basic operations: expansion, erosion, open operation and closed operation. They have their own characteristics in binary images and grayscale images. Based on these basic operations, various practical algorithms of mathematical morphology can be deduced and combined, and they can be used to analyze and process image shapes and structures.

1) EDGE REFINEMENT

The purpose of refinement is to make the width of the edge one pixel. The result of the refinement is called the skeleton of the original image. The skeleton has the same topological shape and connectivity as the original image. Hit-or-miss transformation is the theoretical basis for the marginalization of mathematical morphology. The basic idea of hit-or-miss transformation is to extract all pixels in the image that match a given neighborhood structure.

Let $f(x,y)$ be the input image and $b(x,y)$ be the structural element. $b(x,y)$ is composed of two disjoint parts $b_1(x,y)$ and $b_2(x,y)$, and the intersection of them is an empty set. The union of them forms the structural element. So, the definition of $f(x,y)$ hit by $b(x,y)$ is defined as

$$f * b(x,y) = (f \odot b_1) \cap \left(f^c \odot b_2\right), \tag{17}$$

where $\odot$ represents erosion. Further, we can know that the definition of edge refinement is defined as

$$f \otimes b(x,y) = f - f * b(x,y). \tag{18}$$

Let's set up a series of structural elements as

$$\{b(x,y)\} = \{b_1(x,y), b_2(x,y), \cdots, b_n(x,y)\}. \tag{19}$$

Then, the formula of the image $f(x,y)$ refined by the structural elements is defined as

$$f \otimes \{b\}(x,y) = (\cdots((f \otimes b_1) \otimes b_2) \cdots) \otimes b_n. \tag{20}$$

It can be seen that the refinement process is to first refine the image $f(x,y)$ with a structural element $b_1(x,y)$. Then, $b_2(x,y)$ is used to refine the result of $b_1(x,y)$, and so on, until $b_n(x,y)$ is used to refine the image. The whole process is repeated until the results are no longer changed.

2) ELIMINATE FALSE EDGES

In a binary image, if two pixels with a value of 1 are adjacent, the two pixels can be connected. All the maximal connected blocks are found in the image matrix. The maximal connected block means that the connected block has already contained all adjacent pixels with a value of 1. As shown in Figure 4,

1	1	1	1	1	1	1	1
0	0	0	0	0	0	0	0
1	1	0	0	0	0	1	0
0	1	1	0	0	0	0	1
0	0	0	0	1	0	0	0
0	1	0	1	1	0	0	0
1	1	0	1	1	1	0	1
1	0	0	0	0	0	0	1

FIGURE 4. Maximal connected block.

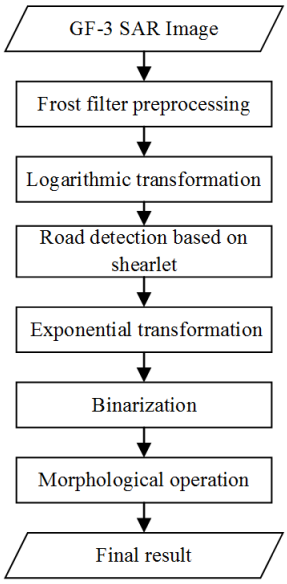

FIGURE 5. Flowchart of road detection.

there are six maximal connected blocks. Each maximal connected block is traversed and the number of pixels in the connected block is calculated. Then, a threshold is set. If the number of pixels in a maximal connected block is less than the threshold, the value of all pixels in the connected block is set to 0, which is equivalent to treating the connected block as a false edge and then removing it.

The above two-step morphological operations are simple and easy to implement. They can refine edges and remove a large number of false edges. Finally, a binary image with few false edges and clear roads is obtained.

In summary, the flowchart of road detection of GF-3 SAR images is shown in Figure 5. Firstly, due to the appearance of speckle in GF-3 SAR images and the characteristics of the weak roads studied in this paper, we use the Frost filter for preprocessing, and try to preserve the useful features of the roads and suppress speckle effectively. Secondly, in order to apply shearlet, the multiplicative speckle model is transformed into additive one by logarithmic transformation. Then, we use even-symmetric shearlet and odd-symmetric

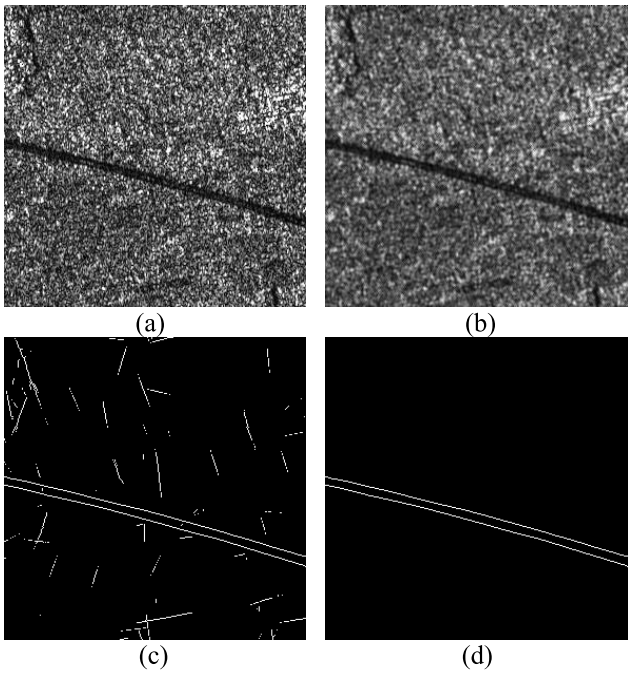

FIGURE 6. Road detection results (a) original image, (b) Frost filter preprocessing, (c) road detection based on shearlet, (d) morphological operation.

shearlet to transform the image and obtain the transformed coefficients. A series of operations on the coefficients are performed to calculate the probability of a road on each pixel of image. Since shearlet has optimal sparsity and strong directional orientation, the detected roads is guaranteed to have high accuracy. Next, the result of the detection is exponentially transformed, and an appropriate threshold is selected for binarization. Lastly, in order to solve the problems of thick edges and false edges, two morphological operations are used, including refinement and removal of false edges, and then the final detected results of road can be obtained.

In a word, the proposed algorithm contains three key points. Firstly, the Frost filter is used for despeckling, which can reduce the impact of speckle on the subsequent road detection. Then, shearlet is used for road detection to get high detecting accuracy. Finally, morphological operations are adopted to refine edges and eliminate false edges to obtain the final result.

V. ROAD DETECTION EXPERIMENTS

In this section, three GF-3 SAR images are used to verify the proposed road detection algorithm.

Figure 6 shows the road detection result of a GF-3 SAR image. We can see that the Frost filter can effectively reduce speckle interference, and road information is effectively preserved. Then, the use of shearlet with optimal sparsity and strong directional orientation can effectively detect roads and ensure the high accuracy, continuity and smoothness of road detection, but there are still a few false edges caused by speckle interference. Then, we use morphological operations to refine edges and remove false edges to obtain the final

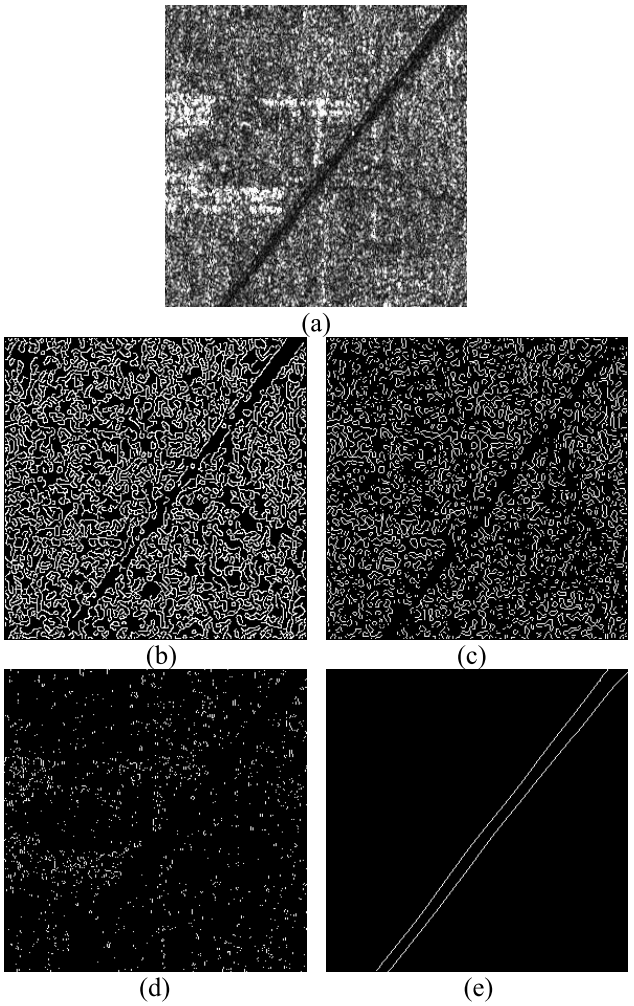

FIGURE 7. Road detection results using different methods: (a) original image, (b) Canny, (c) LoG, (d) Sobel, (e) our method.

detected results. In summary, since shearlet has the optimal sparsity and strong directional localization, the road features of GF-3 SAR images with strong sparse characteristics can be efficiently detected.

Figure 7 shows the road detection result of another GF-3 SAR image, and provides the detection results of the traditional difference operators for comparison. The essence of Canny operator is to use a quasi-Gaussian function to do the smoothing operation, and then use the first-order differential operator with direction to locate the derivative extremum to detect the edges. The essence of LoG operator is to smooth the original image with a Gaussian function, and then use the non-directional Laplacian operator to extract the zero-crossing points for edge detection. Sobel is a differential template operator that uses a template to convolve the image and extract the edges. There is a serious double-edge phenomenon and only partial road information in the Canny operator results. There is a serious rupture in the roads in the LoG operator results, but the roads trend can be barely seen as a whole. The Sobel operator is only a template operator, which causes road information to disappear almost completely. These three

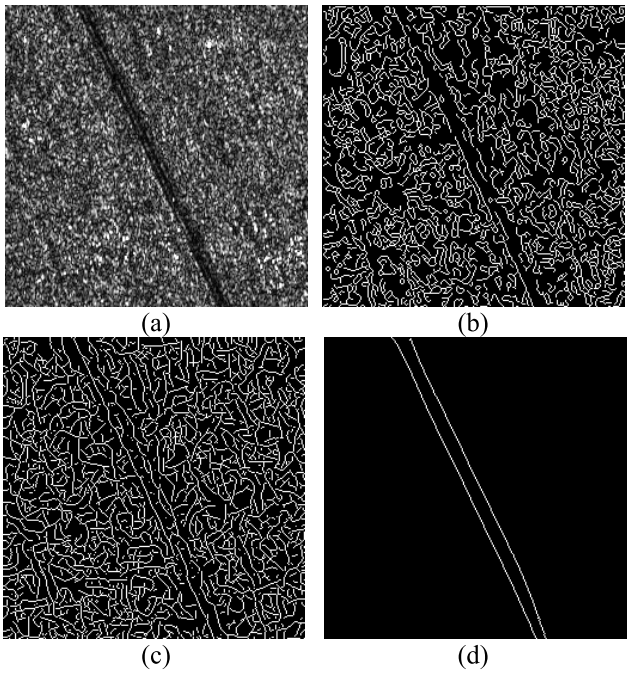

FIGURE 8. Road detection results using different methods: (a) original image, (b) the detector proposed in [41], (c) the detector proposed in [42], (d) our method.

detection methods are based on difference, so the interference of the multiplicative speckle is extremely serious. It can be seen that the traditional three differential operators are not suitable for road detection of GF-3 SAR images, especially the detection of weak roads under strong speckle interference. The proposed method combines the Frost filter, detection based on shearlet and morphological operations. It not only uses the Frost filter to suppress speckle, but also uses the optimal sparsity and strong directional localization of shearlet. Additionally, the proposed method uses morphological operations to refine the results and remove the false edges, leading to the desired detection results of road. In short, the accuracy of the road detection results of the proposed method is high, and the roads detected are complete and smooth. Therefore, the proposed method is very suitable for the detection of the weak road under the strong speckle interference of GF-3 SAR images.

Figure 8 shows the road detection result of the last GF-3 SAR image, and provides the detection results of the methods proposed in [41] and [42] for comparison. The detector proposed in [41] is a noise-robust color edge detector using gradient matrix and anisotropic Gaussian directional derivative matrix. The detector proposed in [42] is a ratio-based edge detector using Gaussian-Gamma-shaped bi-windows. In the detection result of the detector in [41], there are lots of false edges and the road detected is seriously broken. In the detection result of the detector in [42], there are also many false edges but the road detected is complete and smooth in some degree. Compared with our detector, the two latest methods still lead to much more false edges and detected roads with lower smoothness and completeness.

TABLE 2. Qualitative evaluation results of different detectors.

Detectors	Anti-speckle	Completeness	Smoothness
Canny	weak	low	low
LoG	weak	low	low
Sobel	weak	low	low
Detector in [41]	weak	medium	low
Detector in [42]	weak	medium	medium
Our method	strong	high	high

So these two detectors are not suitable for the detection of weak roads under strong speckle interference for GF-3 SAR images. It should be noted that our method which combines the Frost filter, shearlet-based edge detection and morphological operations, is very efficient for detecting weak roads under strong speckle interference.

Table 2 shows the qualitative evaluation results of different detectors. There are three indicators in this table, namely, anti-speckle, completeness and smoothness. Anti-speckle denotes the ability to reduce the influence of speckle on road detection results. This indicator is very important, especially for the detection of weak roads under strong speckle interference. Completeness denotes the clarity of the direction and outline of the detected road as a whole. Smoothness refers to the extent to which the detected road is continuous and does not break. It should be noted that our method is a compound algorithm and includes special designs for strong speck interference such as the combined use of Frost filter and morphological operations. So the ability of anti-speckle of our method is strong. Additionally, the completeness and smoothness of our method are both high, because we detect road information by using shearlet with the optimal sparsity and the strong directional orientation. In a word, owe to several advantages above, our method is very appropriate for the detection of weak roads under strong speckle interference for GF-3 SAR images.

VI. CONCLUSION

The weak roads under strong speckle interference are detected in this paper. Shearlet with optimal sparsity and strong directional orientation is used to construct an efficient detection method for GF-3 SAR images. Firstly, the Frost filter is used for despeckling and the valid road information is preserved effectively. Then, shearlet is used for road detection. Finally, two-step morphological operations are used to refine the detected edges and remove the false edges, and the final road detection results are obtained. The road detection experiments on various GF-3 SAR images demonstrate that, the proposed method can perform well with high detection accuracy, eliminate the false edges caused by speckle, and make the detected roads continuous and smooth. Therefore, our method is indeed an efficient method for road detection under strong speckle interference for GF-3 SAR images.

REFERENCES

[1] J. C. Li, S. X. Huang, and Y. X. Peng, "A novel method to configure the parameters of the bilateral filtering for synthetic aperture radar images speckle reduction," *Acta Phys. Sinica*, vol. 61, no. 11, pp. 9501–9505, Sep. 2012.
[2] R. Reisenhofer, J. Kiefer, and E. J. King, "Shearlet-based detection of flame fronts," *Exp. Fluids*, vol. 57, no. 3, pp. 41–45, Feb. 2016.
[3] A. E. Bayley, Y. Hardalupas, and A. M. K. P. Taylor, "Local curvature measurements of a lean, partially premixed swirl-stabilised flame," *Exp. Fluids*, vol. 52, no. 4, pp. 963–983, Apr. 2012.
[4] X. Ma, S. Liu, S. Hu, P. Geng, M. Liu, and J. Zhao, "SAR image edge detection via sparse representation," *Soft Comput.*, vol. 22, no. 8, pp. 2507–2515, Apr. 2018.
[5] P. Shui and S. Fan, "SAR image edge detection robust to isolated strong scatterers using anisotropic morphological directional ratio test," *IEEE Access*, vol. 6, pp. 37272–37285, 2018.
[6] Y. Xiang, F. Wang, L. Wan, and H. You, "SAR-PC: Edge detection in SAR images via an advanced phase congruency model," *Remote Sens.*, vol. 9, no. 3, p. 209, Feb. 2017.
[7] Q. An, Z. Pan, and H. You, "Ship detection in Gaofen-3 SAR images based on sea clutter distribution analysis and deep convolutional neural network," *Sensors*, vol. 18, no. 2, p. 334, Jan. 2018.
[8] W. Shao, Y. Sheng, and J. Sun, "Preliminary assessment of wind and wave retrieval from Chinese Gaofen-3 SAR imagery," *Sensors*, vol. 17, no. 8, p. 1705, Jul. 2017.
[9] W. Wei, X.-L. Yang, P.-Y. Shen, and B. Zhou, "Holes detection in anisotropic sensornets: Topological methods," *Int. J. Distrib. Sensor Netw.*, vol. 8, no. 10, Oct. 2012, Art. no. 135054.
[10] W. Wei, Y. Qiang, and J. Zhang, "A bijection between lattice-valued filters and lattice-valued congruences in residuated lattices," *Math. Problems Eng.*, vol. 2013, pp. 1–6, Jul. 2013.
[11] H. M. Srivastava, Y. Zhang, P. Shen, J. Zhang, and L. Wang, "A local fractional integral inequality on fractal space analogous to Anderson's inequality," *Abstract Appl. Anal.*, vol. 46, no. 8, pp. 5218–5229, Jun. 2014.
[12] S. Liu, W. Li, W. Wei, and D. Z. Du, "Fractal intelligent privacy protection in online social network using attribute-based encryption schemes," *IEEE Trans. Comput. Social Syst.*, vol. 5, no. 3, pp. 736–747, Sep. 2018.
[13] X. L. Fan, H. B. Song, and L. Wei, "H∞ control of network control system for singular plant," *Inf. Technol. Control*, vol. 47, no. 1, pp. 140–150, Feb. 2018.
[14] Q. Ke, J. Zhang, H. Song, and Y. Wan, "Big data analytics enabled by feature extraction based on partial independence," *Neurocomputing*, vol. 288, pp. 3–10, May 2018.
[15] Q. Ke, J. Zhang, W. Wei, D. Połap, M. Woźniak, L. Kośmider, and R. Damaševičius, "A neuro-heuristic approach for recognition of lung diseases from X-ray images," *Expert Syst. Appl.*, vol. 126, pp. 218–232, Jul. 2019.
[16] Q. Ke, J. Zhang, W. Wei, R. Damasevicius, and M. Wozniak, "Adaptive independent subspace analysis of brain magnetic resonance imaging data," *IEEE Access*, vol. 7, pp. 12252–12261, 2019.
[17] Q. Ke, J. Zhang, W. Wei, and M. Wozniak, "The phase and shift-invariant feature by adaptive independent subspace analysis for cortical complex cells," *Inf. Technol. Control*, vol. 48, no. 1, pp. 58–70, Oct. 2018.
[18] W. Wei, J. Su, H. Song, H. Wang, and X. Fan, "CDMA-based anti-collision algorithm for EPC global C1 Gen2 systems," *Telecommun. Syst.*, vol. 67, no. 1, pp. 63–71, Jan. 2018.
[19] P. Zheng, Y. Qi, Y. Zhou, P. Chen, J. Zhan, and M. R. Lyu, "An automatic framework for detecting and characterizing performance degradation of software systems," *IEEE Trans. Rel.*, vol. 63, no. 4, pp. 927–943, Dec. 2014.
[20] P. Wang, Y. Qi, and X. Liu, "Power-aware optimization for heterogeneous multi-tier clusters," *J. Parallel Distrib. Comput.*, vol. 74, no. 1, pp. 2005–2015, Jan. 2014.
[21] Y.-N. Qiao, Q. Yong, and H. Di, "Tensor field model for higher-order information retrieval," *J. Syst. Softw.*, vol. 84, no. 12, pp. 2303–2313, Dec. 2011.
[22] J. Yan, Y. Qi, and Q. Rao, "Detecting malware with an ensemble method based on deep neural network," *Secur. Commun. Netw.*, vol. 2018, pp. 1–16, Mar. 2018.
[23] X. Wang, Y. Qi, Z. Wang, Y. Chen, and Y. Zhou, "Design and implementation of SecPod, a framework for virtualization-based security systems," *IEEE Trans. Dependable Secure Comput.*, vol. 16, no. 1, pp. 44–57, Jan. 2019.

[24] W. Wei and Y. Qi, "Information potential fields navigation in wireless ad-hoc sensor networks," *Sensors*, vol. 11, no. 5, pp. 4794–4807, May 2011.
[25] W. Wei, X. Fan, H. Song, X. Fan, and J. Yang, "Imperfect information dynamic Stackelberg game based resource allocation using hidden Markov for cloud computing," *IEEE Trans. Serv. Comput.*, vol. 11, no. 1, pp. 78–89, Jan. 2018.
[26] W. Wei, H. Song, W. Li, P. Shen, and A. Vasilakos, "Gradient-driven parking navigation using a continuous information potential field based on wireless sensor network," *Inf. Sci.*, vol. 408, pp. 100–114, Oct. 2017.
[27] W. Wei, Q. Xu, L. Wang, X. H. Hei, P. Shen, W. Shi, and L. Shan, "GI/Geom/1 queue based on communication model for mesh networks," *Int. J. Commun. Syst.*, vol. 27, no. 11, pp. 3013–3029, 2014.
[28] W. Wei, Z. Sun, H. Song, H. Wang, X. Fan, and X. Chen, "Energy balance-based steerable arguments coverage method in WSNs," *IEEE Access*, vol. 6, pp. 33766–33773, 2018.
[29] W. Wei, H. Song, H. Wang, and X. Fan, "Research and simulation of queue management algorithms in ad hoc networks under DDoS attack," *IEEE Access*, vol. 5, pp. 27810–27817, 2017.
[30] W. Wei, X. Fan, H. Song, and H. Wang, "Video tamper detection based on multi-scale mutual information," *Multimedia Tools Appl.*, vol. 78, no. 19, pp. 27109–27126, Oct. 2019.
[31] W. Wei, X.-L. Yang, B. Zhou, J. Feng, and P.-Y. Shen, "Combined energy minimization for image reconstruction from few views," *Math. Problems Eng.*, vol. 2012, pp. 1–15, Oct. 2012.
[32] G. Easley, D. Labate, and W. Q. Lim, "Sparse directional image representation using the discrete Shearlet transform," *Appl. Comput. Harmon. Anal.*, vol. 25, no. 1, pp. 25–46, Jul. 2008.
[33] S. Q. Liu, S. H. Hu, and Y. Xiao, "SAR image de-noising based on complex Shearlet transform domain Guassian mixture model," *Acta Aeronautica et Astronautica Sinica*, vol. 34, no. 1, pp. 173–180, Jan. 2013.
[34] W.-Q. Lim, "The discrete Shearlet transform: A new directional transform and compactly supported Shearlet frames," *IEEE Trans. Image Process.*, vol. 19, no. 5, pp. 1166–1180, May 2010.
[35] G. Kutyniok and D. Labate, *Shearlets: Multiscale Analysis for Multivariate Data*, 1st ed. Basel, Switzerland: Birkhäuser, 2012, pp. 30–31.
[36] L. Zhu, T. Q. Han, and P. L. Shui, "An anisotropic diffusion filtering method for speckle reduction of synthetic aperture radar images," *Acta Phys. Sinica*, vol. 63, no. 17, pp. 9502–9511, Sep. 2014.
[37] Z. G. Sun and C. Z. Han, "Modeling high-resolution synthetic aperture radar images with heavy-tailed distribution," *Acta Phys. Sinica*, vol. 59, no. 2, pp. 998–1008, Feb. 2010.
[38] R. Reisenhofer, "The complex shearlet transform and applications to image quality assessment," M.S. thesis, Dept. Math., Technische Universität Berlin, Berlin, Germany, 2014.
[39] E. J. King, R. Reisenhofer, J. Kiefer, W.-Q. Lim, Z. Li, and G. Heygster, "Shearlet-based edge detection: Flame fronts and tidal flats," *Proc. SPIE, Appl. Digit. Image Process. XXXVIII*, vol. 9599, Sep. 2015, Art. no. 959905.
[40] I. Selesnick, "Hilbert transform pairs of wavelet bases," *IEEE Signal Process. Lett.*, vol. 8, no. 6, pp. 170–173, Jun. 2001.
[41] F.-P. Wang and P.-L. Shui, "Noise-robust color edge detector using gradient matrix and anisotropic Gaussian directional derivative matrix," *Pattern Recognit.*, vol. 52, pp. 346–357, Apr. 2016.
[42] P.-L. Shui and D. Cheng, "Edge detector of SAR images using Gaussian-gamma-shaped bi-windows," *IEEE Geosci. Remote Sens. Lett.*, vol. 9, no. 5, pp. 846–850, Sep. 2012.

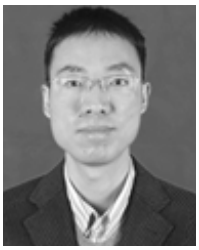

ZENGGUO SUN was born in Xi'an, Shaanxi, China, in 1980. He received the bachelor's degree in computer science and technology and the Ph.D. degree in control science and engineering from Xi'an Jiaotong University, in 2003 and 2010, respectively. He was a Visiting Scholar with Pennsylvania State University, from 2007 to 2008. He is currently an Associate Professor with Shaanxi Normal University. His research interest includes radar image processing.

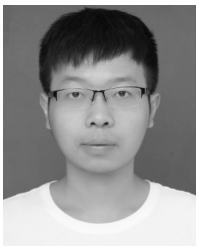

DEDAO LIN was born in Wenzhou, Zhejiang, China, in 1995. He received the bachelor's degree in software engineering from Zhengzhou University, in 2018. He is currently pursuing the master's degree in computer technology with Shaanxi Normal University. His research interest includes radar image processing.

WEI WEI (Senior Member, IEEE) received the M.S. and Ph.D. degrees from Xi'an Jiaotong University, Xi'an, China, in 2005 and 2011, respectively. He is currently an Associate Professor with the School of Computer Science and Engineering, Xi'an University of Technology, Xi'an. He ran many funded research projects as a Principal Investigator and Technical Member. He has published over 100 research articles in international conferences and journals. His current research interests include the area of wireless networks, wireless sensor networks application, image processing, mobile computing, distributed computing, and pervasive computing, the Internet of Things, and sensor data clouds. He is a Senior Member of the China Computer Federation. He is an Editorial Board Member of the *Future Generation Computer System*, the IEEE Access, *Ad Hoc & Wireless Sensor Network*, *Institute of Electronics, Information and Communication Engineers*, and *KSII Transactions on Internet and Information Systems*. He is a TPC member of many conferences and also a regular Reviewer of the IEEE Transactions on Parallel and Distributed Systems, the IEEE Transactions on Image Processing, the IEEE Transactions on Mobile Computing, the IEEE Transactions on Wireless Communications, *Journal of Network and Computer Applications*, and many other Elsevier journals.

MARCIN WOŹNIAK received the Diploma degree in applied mathematics and computational intelligence. He is currently an Associate Professor with the Institute of Mathematics, Silesian University of Technology, Gliwice, Poland. His main scientific interest is neural networks with their applications together with various aspects of applied computational intelligence. He is a Scientific Supervisor in editions of the "Diamond Grant" and "The Best of the Best" programs for highly talented students from the Polish Ministry of Science and Higher Education. He served as an editor for various special issues, and as an organizer or the session chair at various international conferences and symposiums.

ROBERTAS DAMAŠEVIČIUS received the B.Sc. degree in informatics from the Faculty of Informatics, Kaunas University of Technology (KTU), Kaunas, Lithuania, in 1999, and the M.Sc. degree *(cum laude)* in 2001. He defended his Ph.D. thesis at KTU, in 2005. He is currently a Professor with the Software Engineering Department, KTU, where he lectures robot programming and software maintenance courses. He is the author or coauthor of over 100 articles as well as a monograph published by Springer. His research interests include brain–computer interface, bioinformatics, data mining, and machine learning.